

See discussions, stats, and author profiles for this publication at: <https://www.researchgate.net/publication/38069098>

# Fragment 101–108 of Myelin Oligodendrocyte Glycoprotein: A Possible Lead Compound for Multiple Sclerosis

ARTICLE in JOURNAL OF THE AMERICAN CHEMICAL SOCIETY · NOVEMBER 2009

Impact Factor: 12.11 · DOI: 10.1021/ja905154j · Source: PubMed

---

CITATIONS

3

READS

26

## 4 AUTHORS:



[Carlo Guardiani](#)

Università degli studi di Cagliari

30 PUBLICATIONS 112 CITATIONS

[SEE PROFILE](#)



[Simone Marsili](#)

Centro Nacional de Investigaciones Oncoló...

22 PUBLICATIONS 307 CITATIONS

[SEE PROFILE](#)



[Piero Procacci](#)

University of Florence

117 PUBLICATIONS 2,080 CITATIONS

[SEE PROFILE](#)



[Roberto Livi](#)

University of Florence

182 PUBLICATIONS 3,836 CITATIONS

[SEE PROFILE](#)

## Fragment 101–108 of Myelin Oligodendrocyte Glycoprotein: A Possible Lead Compound for Multiple Sclerosis

Carlo Guardiani,<sup>\*†</sup> Simone Marsili,<sup>‡</sup> Piero Procacci,<sup>‡</sup> and Roberto Livi<sup>†§</sup>

*Centro Interdipartimentale per lo Studio delle Dinamiche Complesse (CSDC), Università di Firenze, Italy, Laboratorio di Spettroscopia Molecolare, Dipartimento di Chimica, Università di Firenze, Italy, and Dipartimento di Fisica, Università di Firenze, Sezione INFN di Firenze e INFN UdR Firenze, Italy*

Received June 23, 2009; E-mail: guardiani@fi.infn.it

**Abstract:** Multiple Sclerosis (MS) is a highly invalidating autoimmune disease of the Central Nervous System, leading to progressive paralysis and, sometimes, to premature death. One of the potential targets of the autoimmune reaction is the myelin protein MOG (Myelin Oligodendrocyte Glycoprotein). Since the 101–108 fragment of MOG plays a key role in the interaction with the MS-autoantibody 8-18C5, we performed an analysis of the equilibrium conformations of this peptide using the Replica Exchange Molecular Dynamics technique in conjunction with the Generalized Born continuum solvent model. Four variants of the peptide, stabilized by a disulfide bond, were also studied. We found that a significant fraction of the equilibrium population retains the original  $\beta$ -hairpin conformation, and the amount of crystal-like conformations increases in the disulfide-closed analogues. When the equilibrium structures were used in docking simulations with the 8-18C5 antibody, we discovered the existence of a docking funnel whose bottom is populated by stable complexes where the peptide occupies the same region of space that was occupied in the crystal. It follows that the MOG 101–108 fragment represents a promising starting point for the design of a drug capable of blocking the 8-18C5 antibody. The molecule may also be used for the development of a diagnostic assay for multiple sclerosis.

### 1. Motivation

Multiple Sclerosis (MS) is a chronic autoimmune disease of the Central Nervous System characterized by aggressive T and B cell responses leading to the destruction of the myelin sheath that electrically insulates the axons, which determines a condition of progressive paralysis and disability in a population of young adults, in the most productive period of life (20–50 years of age).

One of the most important targets of the autoimmune attack is the protein MOG, which being placed on the outermost layer of the myelin sheath is vulnerable to the antibodies present in the extracellular medium. The importance of MOG in the pathogenesis of MS is supported by the observation that it is the only antigen capable of eliciting both a B<sup>1</sup> and a T-cell<sup>2</sup> response. Moreover, MOG-specific antibodies have been identified in actively demyelinating lesions of MS patients.<sup>3</sup>

A series of experiments performed by Linington and co-workers<sup>4,5</sup> showed that MOG-specific monoclonal antibodies,

despite being capable of interacting with the full extracellular domain of MOG, fail to recognize a panel of overlapping 15-mer and 25-mer MOG peptides. This led to the conclusion that MOG antibodies only recognize discontinuous epitopes. This result, however, seems to be in disagreement with the structure of the crystal complex of MOG<sup>IgD</sup> with the Fab of the MOG-specific monoclonal antibody 8-18C5, recently resolved through X-ray diffraction by Breithaupt and co-workers.<sup>6</sup>

In fact, as shown in Figure 1, MOG<sup>IgD</sup> (Extracellular, Ig-like domain of Myelin Oligodendrocyte Glycoprotein) mainly interacts with the heavy chain of the 8-18C5 antibody, using the FG loop, which corresponds to residues 101–108. This fragment, which provides 65% of the interaction surface of MOG with the antibody, is completely buried in a pocket delimited by the CDRs H1–H3. In particular, while residues Asp102, His103, and Ser104 are located at the bottom of the cavity where they establish polar and hydrophobic interactions with H3, Ser104 and Gln106 form a short intermolecular  $\beta$ -sheet by H-bonding residues Ser31 and Trp33 of the CDR H1. The complex is further stabilized by the hydrogen bonds that Glu107 and Glu108 establish with the H2 residues Arg54 and Arg56. It could be therefore suggested that the absence of antibody/peptide interactions observed by Linington is the result of the large size

<sup>†</sup> CSDC.

<sup>‡</sup> Dipartimento di Chimica.

<sup>§</sup> Dipartimento di Fisica.

- (1) Lebar, R.; Lubetzki, C.; Vincent, C.; Lombrail, P.; Boutry, J. M. *Clin. Exp. Immunol.* **1986**, *66*, 423–434.
- (2) Amor, S.; Groome, N.; Linington, C.; Morris, M. M.; Dormmair, K.; Gardinier, M. V.; Matthieu, J. M.; Baker, D. *J. Immunol.* **1994**, *153*, 4349–4356.
- (3) Genain, C. P.; Cannella, B.; Hauser, S. L.; Raine, C. S. *Nat. Med.* **1999**, *5*, 170–175.
- (4) Brehm, U.; Piddesden, S. J.; Gardinier, M. V.; Linington, C. *J. Neuroimmunol.* **1999**, *97*, 9–15.
- (5) Haase, C. G.; Guggenmos, J.; Brehm, U.; Andersson, M.; Olsson, T.; Reindl, M.; Schneidewind, J. M.; Zettl, U. K.; Heidenreich, F.; Berger, T.; Wekerle, H.; Hohlfeld, R.; Linington, C. *J. Neuroimmunol.* **2001**, *114*, 220–225.
- (6) Breithaupt, C.; Schubert, A.; Zander, H.; Skerra, A.; Huber, R.; Linington, C.; Jacob, U. *Proc. Natl. Acad. Sci. U.S.A.* **2003**, *100*, 9446–9451.

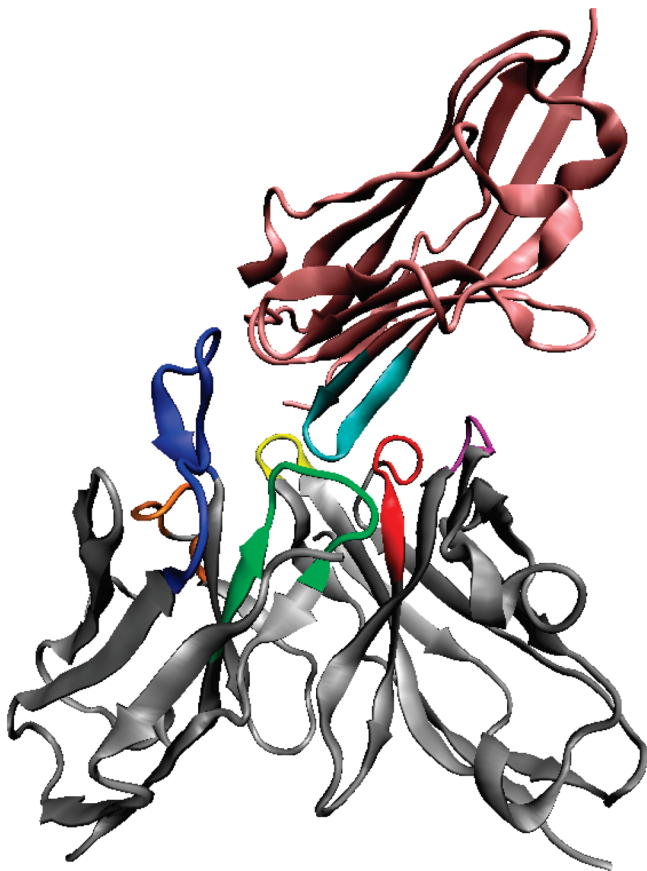


**Figure 1.** Crystal complex of the extracellular domain of rat MOG (in pink) with the variable domains of the 8-18C5 antibody (PDB-ID:1PKQ). The Complementarity Determining Regions are highlighted in color: L1, blue; L2, orange; L3, green; H1, red; H2, magenta; H3, yellow. MOG 101–108 fragment, displayed in cyan, is completely buried in the binding pocket of the antibody, and it mainly interacts with the variable domain of the heavy chain (on the right).

of the peptides, which might therefore fold in a structure incompatible with the shape of the binding site of the 8-18C5 antibody. This study aims at determining if the fragment MOG 101–108 retains the ability of recognizing the binding pocket of the 8-18C5 antibody.

Our work is mainly based on Molecular Dynamics (MD) and docking simulations. The computational approach, being rather fast and inexpensive, may suggest interesting directions where the labor-intensive experimental analysis should be addressed. Docking simulations have been performed with the HADDOCK software<sup>7</sup> that turned out to be extremely reliable in many problems of protein/peptide<sup>8,9</sup> and protein/protein<sup>10,11</sup> recognition. This is due to the excellent parametrization of the nonbonded interactions derived from the OPLS<sup>12</sup> force field and

to a sophisticated docking protocol organized in three steps: (i) randomization of orientations and rigid body energy minimization, (ii) semiflexible simulated annealing in torsion angle space, and (iii) final refinement in explicit solvent.

Docking simulations, however, cannot be directly performed, since the equilibrium conformations of the 101–108 peptide are not known when the fragment is excised from MOG<sup>1gd</sup>. To retrieve this information we performed Molecular Dynamics simulations. MD simulations of peptides and proteins are quite challenging, since the conformational space is highly dimensional and the energy landscape is extremely rugged, with a huge number of local minima where the peptide may remain trapped during the simulation. To overcome such sampling limitations of standard MD, several computational techniques have been developed.<sup>13–15</sup> In this study we have used the parallel tempering technique, also known as replica exchange and originally introduced for the study of disordered spin systems.<sup>16,17</sup> Sugita and Okamoto extended this technique into a version suitable for MD simulations that they called REMD (Replica Exchange Molecular Dynamics).<sup>18</sup> In an REMD simulation,  $N$  copies of the system are simulated in parallel at different temperatures, and at regular time intervals,  $N/2$  temperature exchanges of replicas at neighboring temperatures are attempted. Exchanges are accepted or rejected according to a Metropolis-like criterion that satisfies the detailed balance principle. In particular, the probability of accepting a temperature exchange between replicas  $i$  and  $j$  is computed as  $p_{ij} = \min(1, \exp(-\Delta))$  where  $\Delta = (\beta_i - \beta_j)(E_j - E_i)$  and  $\beta = 1/k_B T$ ,  $T$  being the temperature and  $E$  the potential energy of the system. In extreme synthesis, the advantage of this technique is that the acquisition of hot configurations that may result from the exchanges allows the peptide to escape from a configurational trap where it was stuck, thereby greatly enhancing the efficiency of the sampling at the target physiological temperature.

A well-known limit of the REMD technique in the simulation of proteins in explicit solvent is the fine grained spacing of the replicas in the temperature space needed for acceptable exchange probability,<sup>19</sup> with most of the extra heat from hot replicas spent in exchanging uninteresting configurations (e.g., solvent configurations). This problem can be overcome by using an implicit solvent approach such as the Generalized Born (GB) model. MD simulations using the GB model are inherently less expensive than the explicit solvent simulations. Moreover, in the context of the REMD technology, the use of implicit models straightforwardly implies the tempering of the solute only, thus allowing for a coarser sampling of the replica in the temperature space without degrading the acceptance probability of exchanges. A family of particularly fast GB models<sup>20</sup> is based on integration over the internal volume of the protein, approximated as a set of atom spheres. The tendency of these models to overestimate the volume of the internal water-filled cavities was

- (7) Dominguez, C.; Boelens, R.; Bonvin, A. M. J. J. Am. Chem. Soc. **2003**, *125*, 1731–1737.
- (8) Mahadev, R. K.; Di Pietro, S. M.; Olson, J. M.; Piao, H. L.; Payne, G. S.; Overduin, M. EMBO J. **2007**, *26*, 1963–1971.
- (9) Wei, Y.; Liu, S.; Lausen, J.; Woodrell, C.; Cho, S.; Biris, N.; Kobayashi, N.; Wei, Y.; Yokoyama, S.; Werner, M. H. Nat. Struct. Mol. Biol. **2007**, *14*, 653–661.
- (10) Lin, Z.; Sriskanthadevan, S.; Huang, H.; Siu, C. H.; Yang, D. Nat. Struct. Mol. Biol. **2006**, *13*, 1016–1022.
- (11) Liew, C. K.; Simpson, R. J. Y.; Kwan, A. H. Y.; Crofts, L. A.; Loughlin, F. E.; Matthews, J. M.; Crossley, M.; Mackay, J. P. Proc. Natl. Acad. Sci. U.S.A. **2005**, *102*, 583–588.
- (12) Jorgensen, W. L.; Tirado-Rives, J. J. Am. Chem. Soc. **1988**, *110*, 1657–1666.
- (13) Berne, B. J.; Straub, J. E. Curr. Opin. Struct. Biol. **1997**, *7*, 181–189.
- (14) Mitsutake, A.; Sugita, Y.; Okamoto, Y. Biopolymers **2001**, *60*, 96–123.
- (15) Rathore, N.; Knotts, T. A. IV; de Pablo, J. J. J. Chem. Phys. **2003**, *118*, 4285–4290.
- (16) Marinari, E.; Parisi, G. Europhys. Lett. **1992**, *19*, 451–458.
- (17) Marinari, E.; Parisi, G.; Ruiz-Lorenzo, J. J. In *Spin Glasses and Random Fields*; Young, A. P., Ed.; World Scientific: Singapore, 1998; pp 59–98.
- (18) Sugita, Y.; Okamoto, Y. Chem. Phys. Lett. **1999**, *314*, 141–151.
- (19) Liu, P.; Kim, B.; Friesner, R. A.; Berne, B. J. Proc. Natl. Acad. Sci. U.S.A. **2005**, *102*, 13749–13754.
- (20) Bashford, D.; Case, D. A. Annu. Rev. Phys. Chem. **2000**, *51*, 129–152.

corrected in the implementation of Mongan et al.,<sup>21</sup> and when the model was tested on the deca-alanine benchmark, it proved capable of reproducing conformational ensembles in agreement with experimental data.<sup>21,22</sup> The good performance of the model led us to use it for our REMD simulations of the MOG 101–108 peptide. However, as the literature reports a tendency of GB models to overstabilize salt bridges<sup>23</sup> and to introduce a bias toward  $\alpha$ -helices,<sup>24</sup> we also performed simulations in explicit water that are detailed in the Supporting Information. In extreme synthesis, our simulations in explicit solvent are in good agreement with the implicit solvent ones, thus validating our computational protocol.

The organization of our work, described in the following sections, can be summarized as follows. We first performed an alanine-scanning computation of the MOG<sup>lgd</sup>/8-18C5 complex that confirmed the importance of the MOG 101–108 fragment. We then performed docking simulations using the 101–108 fragment excised from MOG<sup>lgd</sup> and kept in a crystal-like conformation. As the crystal fragment proves capable of recognizing the binding pocket of the 8-18C5 antibody, we performed REMD simulations showing that a significant fraction of the equilibrium population of the 101–108 peptide retains a crystal-like structure. The fraction of crystal-like structures was further increased through the design of analogues of the 101–108 peptide constrained in a  $\beta$ -hairpin conformation through a disulfide bond. We finally performed docking simulations using representative conformations of the most populated clusters of the equilibrium population. We attained a significant fraction of low-energy crystal-like complexes suggesting a potential use of the MOG 101–108 peptide as a therapeutic or diagnostic tool for multiple sclerosis.

## 2. Results

**2.1. Alanine Scanning.** An Alanine Scanning Computation was realized on the complex MOG<sup>lgd</sup>/8-18C5 to verify the importance of the 101–108 fragment. All calculations were performed using the free web server <http://robetta.bakerlab.org/alaninescan> implementing the method developed by Kortemme and Baker.<sup>25</sup> In this method, each interface residue is mutated on the turn to Ala and the neighboring residues (within 5 Å of the mutated amino acid) are then reoriented through a Monte Carlo procedure with moves consisting of rotamer–rotamer shifts. The difference  $\Delta\Delta G_{bind}$  between the free energies of binding of the mutant and wild type complexes is then computed. As shown in Table 1, five of the eight residues of fragment 101–108 have a  $\Delta\Delta G_{bind}$  higher than 1 Kcal/mol and can be therefore classified as *hot spots*. The fragment under examination thus appears to play a key role in the stability of the complex.

**2.2. Crystal Docking.** To test the ability of fragment 101–108 to recognize the binding pocket of the antibody, the fragment has been excised from MOG<sup>lgd</sup> and used for docking simulations with 8-18C5. The crystallographic information of the MOG<sup>lgd</sup>

**Table 1.** Alanine Scanning Computation of MOG<sup>lgd</sup> Residues at the Interface with the 8-18C5 Antibody

| Residue | $\Delta\Delta G_{bind}$<br>(kcal/mol) | Residue       | $\Delta\Delta G_{bind}$<br>(kcal/mol) |
|---------|---------------------------------------|---------------|---------------------------------------|
| Gln2    | 0.35                                  | <b>Arg101</b> | <b>1.82</b>                           |
| Lys30   | -0.29                                 | Asp102        | -0.19                                 |
| Thr33   | 0.16                                  | <b>His103</b> | <b>1.78</b>                           |
| Met35   | 0.04                                  | Ser104        | -0.15                                 |
| Tyr40   | 0.55                                  | <b>Tyr105</b> | <b>1.43</b>                           |
| Ser45   | 0.38                                  | <b>Gln106</b> | <b>3.90</b>                           |
| Asn53   | 0.52                                  | Glu107        | 0.25                                  |
|         |                                       | <b>Glu108</b> | <b>1.06</b>                           |

8-18C5 complex cannot be used to define the binding site since *a priori* we do not know if the free fragment binds to the antibody in the same way as when it was part of the full MOG<sup>lgd</sup> domain. The binding site was therefore defined as being composed of the six hypervariable loops (CDRs) of 8-18C5 (see Materials and Methods), keeping the simulation as unbiased as possible. During the run, a moderate flexibility has been allowed both to the CDR loops and to the 101–108 peptide and HADDOCK defines ambiguous interaction restraints (AIR) by randomly picking solvent-exposed residues of the semiflexible regions.

The existence of a docking funnel is the typical signature of the ability of a ligand to interact with a macromolecule. In fact, the structures populating the bottom of the funnel identify a single, specific binding region on the surface of the macromolecule. Figure 2 shows a cloud of points representing the 200 structures produced by the docking simulation.

For each structure we report the intermolecular interaction energy (sum of the van der Waals and electrostatic contributions) as a function of the  $RMSD_{bi}$  (Root Mean Square Deviation of backbone interface atoms) from the minimum energy structure. The computation of  $RMSD_{bi}$  requires the superposition of the backbones of the CDRs of the two structures, and the value is then computed considering the backbone atoms of the full interface composed by the CDRs and the 101–108 peptide. Structural families have been identified using a Quality Threshold clustering method<sup>26</sup> with a cutoff of 12.5 Å, and the average interaction energies of the clusters have been plotted as a

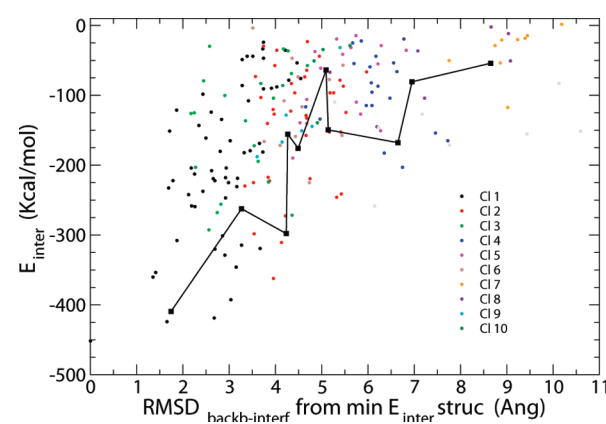


**Figure 2.** Scatterplot of energy vs distance from the minimum energy conformation for the structures produced when docking the MOG 101–108 crystal to the 8-18C5 antibody. The solid curve refers to the average energy and  $RMSD_{bi}$  of the clusters that appear in different colors. Averages are computed over the five lowest-energy structures of each cluster. For the sake of graphical clarity, clusters 11 to 16 that include less than five structures are all shown in gray. As the energy decreases with decreasing values of  $RMSD_{bi}$ , the plot reveals the existence of a docking funnel.

- (21) Mongan, J.; Simmerling, C.; McCammon, A.; Case, D. A.; Onufriev, A. *J. Chem. Theory Comput.* **2007**, *3*, 156–169.
- (22) Roe, D. R.; Okur, A.; Wickstrom, L.; Hornack, V.; Simmerling, C. *J. Phys. Chem. B* **2007**, *111*, 1846–1857.
- (23) Geney, R.; Layten, M.; Gomperts, R.; Hornak, V.; Simmerling, C. *J. Chem. Theory Comput.* **2006**, *2*, 115–127.
- (24) Zhou, R. *Proteins: Struct., Funct., Genet.* **2003**, *53*, 148–161.
- (25) Kortemme, T.; Baker, D. *Proc. Natl. Acad. Sci. U.S.A.* **2002**, *99*, 14116–14121.
- (26) Heyer, L. J.; Kruglyak, S.; Yoosheph, S. *Genome Res.* **1999**, *9*, 1106–1115.

function of the average  $RMSD_{bi}$ . Following ref 27, only clusters including at least five structures are considered, and averages have been computed over the five lowest-energy structures. The plot in Figure 2 shows that moving closer and closer to the minimum-energy structure, the average energy tends to decrease, clearly revealing the existence of a docking funnel. In particular, the cluster with the lowest average  $RMSD_{bi}$  also exhibits the lowest average energy and it also includes the lowest-energy structure of the whole population. The existence of a docking funnel does not necessarily imply that the 101–108 fragment exactly binds in the same crystallographic position and orientation. A simple test to verify this issue is to plot the  $RMSD_{bi}$  from the minimum energy structure ( $R_e$ ) versus the  $RMSD_{bi}$  from the crystal ( $R_c$ ). In the optimal case, where the minimum energy structure exactly coincides with the crystal, all points should lie on the line  $R_e = R_c$ . A linear correlation analysis yielded a regression line of equation  $R_e = 0.73R_c + 0.95$  with a linear correlation coefficient of  $r = 0.76$ , therefore suggesting that the bottom of the docking funnel is populated by crystal-like structures. It can be therefore concluded that if fragment 101–108 is excised from MOG<sup>IgD</sup> and kept in a crystal-like conformation, it retains the capacity to fit into the binding pocket of the 8-18C5 antibody in a crystal-like orientation. We can therefore suggest the following working hypothesis that we are going to check in the following sections: if the 101–108 peptide retains a crystal-like conformation after equilibration under physiological conditions, then it should be capable of recognizing the binding site of the 8-18C5 antibody.

### 2.3. REMD Runs of Free Peptide and SS-Closed Analogues.

The conformational distribution of the MOG 101–108 peptide at equilibrium under physiological conditions was studied through an REMD simulation with 12 replicas, at temperatures chosen in geometric progression<sup>28</sup> ( $T = 310, 332, 355, 380, 406, 435, 465, 498, 533, 570, 610, 652$  K). The simulation, starting with the peptide in the extended conformation, was performed using the GB model described in ref 21 with a Debye–Hückel screening parameter corresponding to a concentration 0.2 M of monovalent ions. For each replica, the first 2 ns of the REMD simulation were discarded, and analysis was performed on 1000 structures sampled at regular time intervals from the following 30 ns of the replica at  $T = 310$  K. Figure 3 shows that a significant fraction of the equilibrium population is crystal-like: 20% of the structures are within 2.5 Å, and 50% of structures are within 3.0 Å  $RMSD_{backb}$  (Root Mean Square Deviation of backbone atoms) from the crystal.

The fraction of crystal-like conformations can be increased by introducing a disulfide bond that forces the peptide to retain the original  $\beta$ -hairpin conformation. For clarity, residues 101–108 are here renumbered from 1 to 8. As in the 101–108 crystal *Gln*6 is just opposite *Arg*1, a straightforward solution amounts to mutating these two residues into *Cys* and link them with a disulfide bridge. Peptide SS16 that results from this design strategy, however, is not expected to bind to the 8-18C5 antibody in the crystallographic orientation. In fact, according to the alanine scanning data reported in Table 1, *Gln*6 and *Arg*1 feature the highest  $\Delta\Delta G_{bind}$ , and therefore the design procedure of SS16 destroys the side chains of the two residues potentially expected to provide the largest contribution to the peptide/antibody

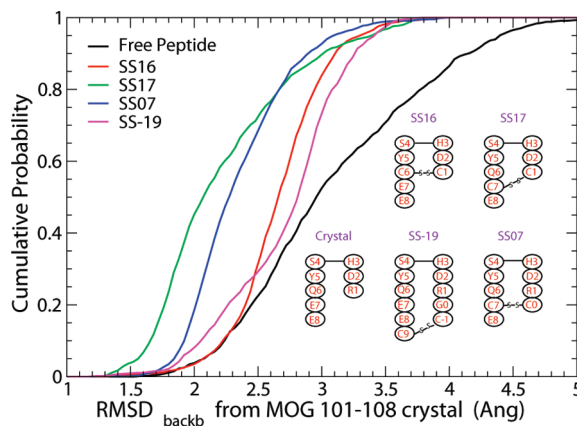


**Figure 3.** Cumulative probability distribution of  $RMSD_{backb}$  from the crystal fragment MOG 101–108 of the equilibrium population at  $T = 310$  K of the peptides analyzed in this work. The disulfide-linked peptides (whose schematic representation is also given) are more crystal-like than the free peptide.

interaction energy. This problem is partly alleviated in peptide SS17 where the disulfide bond is placed in position 1–7. This approach still eliminates the side chain of *Arg*1, but at least it saves *Gln*6 that has the highest  $\Delta\Delta G_{bind}$ . The loss of the side chain of *Glu*7, conversely, is not particularly significant, since the  $\Delta\Delta G_{bind}$  of this residue is very small. In peptide SS07 we added an extra cysteine in position zero that was linked to *Cys*7 with a disulfide bond. Thus the side chains of both *Arg*1 and *Gln*6 are retained. Finally, in compound SS-19, we added an extra glycine in position zero and an extra cysteine in position –1 that was linked to another supplementary cysteine in position 9. This strategy allows us to retain the side chains of all eight residues of the original peptide.

The SS-closed peptides underwent REMD simulations with the same protocol described for the free peptide. Figure 3 shows the cumulative probability distributions of  $RMSD_{backb}$  from the crystal fragment of all our peptides. The greater steepness of the plots of the SS-linked peptides simply reflects the stiffness of these molecules that can explore only a small portion of the conformational space. As expected, all the peptides with the disulfide bridge are more crystal-like than the free peptide. In particular, SS17 is the most crystal-like compound, while SS16 is not close to the crystal structure. This pattern can be easily explained if we consider that the distance between the  $C_\alpha$  of *Arg*1 and *Gln*6 in our crystal is 4.22 Å, while the distance between the  $C_\alpha$  of two disulfide-bonded cysteines is ~6.15 Å. As a result, the introduction of a disulfide bond in position 1–6 divaricates the  $\beta$ -strands and introduces a large structural deformation that explains the poor crystal similarity of SS16. Conversely, the  $C_\alpha$ – $C_\alpha$  distance of the couple *Arg*1–*Glu*7 is 6.83 Å, which is not much larger than 6.15 Å. It follows that the introduction of an SS-bond in position 1–7 only introduces a small deformation justifying the high crystal similarity of SS17.

**2.4. Docking Simulations of Equilibrated Peptides.** The equilibrium populations at  $T = 310$  K produced by the REMD simulations were clustered using a Quality Threshold technique<sup>26</sup> with a cutoff of 3.0 Å. The metrics used for the clustering was the commonly employed rmsd of backbone atoms. However, this measure may not be appropriate when short peptides are considered. We therefore tested different metrics based on dihedral angles, internal distances and native contacts, discovering a significant robustness of the clustering with respect to the

(27) van Dijk, A. D. J.; Ciofi-Baffoni, S.; Banci, L.; Boelens, R.; Bonvin, A. M. J. J. *J. Proteome Res.* **2007**, 6, 1530–1539.

(28) Kofke, D. A. *J. Chem. Phys.* **2002**, 117, 6911–6914.

(29) Hornak, V.; Abel, R.; Okur, A.; Strockbine, B.; Roitberg, A.; Simmerling, C. *Proteins: Struct., Funct., Bioinf.* **2006**, 65, 712–725.

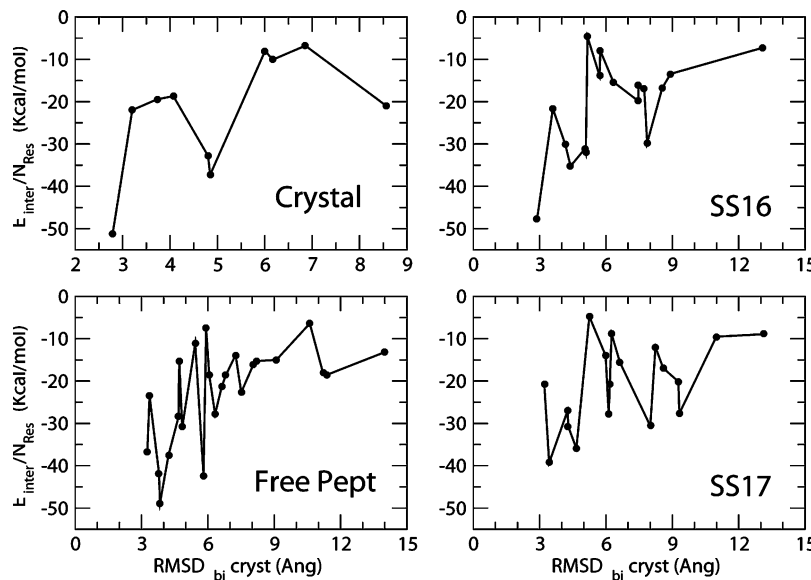


**Figure 4.** Intermolecular energies per residue versus  $RMSD_{bi}$  from the crystal complex MOG101-108/8-18C5. Both quantities are cluster averages computed over the five lowest-energy structures. The four panels refer to the docking simulations using the MOG 101–108 crystal fragment, the free peptide, and the disulfide-closed compounds SS16 and SS17.

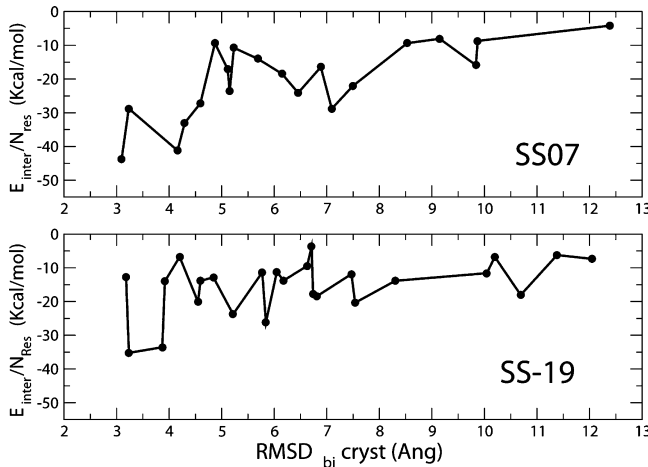


**Figure 5.** Continuation of Figure 4. The two panels refer to the docking simulations using the disulfide-closed compounds SS07 and SS-19.

metrics. A more detailed discussion can be found in the Supporting Information. The structures closest to the centroids of the three most populated clusters were used as input for docking simulations with the 8-18C5 antibody, using the same protocol used for the docking of the crystal fragment. To compare the ability of the peptides to recognize the crystallographic binding site, the 200 structures produced by the HADDOCK run were clustered using the Quality threshold algorithm with a cutoff of 12.5 Å, and the average interaction energy of each cluster was plotted as a function of the average  $RMSD_{bi}$  from the crystal complex (see Figures 4 and 5).

These plots also provide information about the docking funnel since, for all peptides, the structural distance from the crystal correlates well with the  $RMSD_{bi}$  from the minimum energy docking pose, as summarized in Table 2.

As we compare peptides of different lengths, and as energies are a sum of atomic pairwise contributions, in Figures 4 and 5 the interaction energy has been normalized to the number of residues. Thus the energy becomes a measure of the structural fit of the peptide into the binding site of the antibody. Once

**Table 2.** Correlation Analysis of the Docking Simulations:  $RMSD_{bi}$  from Minimum Energy Structure vs  $RMSD_{bi}$  from Crystal

| Peptide    | Regr. Line             | r    |
|------------|------------------------|------|
| Free Pept. | $R_e = 0.84R_c + 0.91$ | 0.91 |
| SS16       | $R_e = 0.98R_c - 0.40$ | 0.94 |
| SS17       | $R_e = 0.99R_c - 0.29$ | 0.97 |
| SS07       | $R_e = 0.68R_c - 2.42$ | 0.76 |
| SS-19      | $R_e = 0.91R_c + 0.31$ | 0.94 |

again, following ref 27 only clusters including at least five structures have been considered, and averages have been computed over the five lowest-energy docking poses of each cluster.

The results of the docking simulation with the crystal fragment 101–108 can be used as a reference to assess the binding capability of the other peptides. In particular, in the reference case, the clusters never exceed a structural distance from the crystal complex of 8.5 Å, and the most crystal-like cluster ( $R_c = 2.79$  Å) is very stable, with an average interaction energy of −51.17 Kcal/mol per residue. The docking performance of the equilibrated peptides is obviously worse, with clusters up to 13.5 Å away from the crystal complex and energies of the most crystal-like cluster reaching ∼−50 Kcal/mol only in the case of the free peptide and of SS16. However, in all the plots of Figures 4 and 5 the energy roughly decreases with the structural distance from the crystal, thus suggesting the existence of a docking funnel with a bottom populated by crystal-like structures. The plots also show that, while in the case of SS16 and SS07 the most crystal-like cluster also features the lowest energy, in the case of SS17, SS-19, and the free peptide, the cluster most similar to the crystal does not have the lowest energy but is nevertheless structurally close to the most stable cluster.

Figure 6 shows the lowest-energy structures of the clusters with the average lowest energy superposed to the crystal complex MOG101–108/8-18C5 so as to minimize the  $RMSD_{backb}$  of the CDR loops of the two antibody molecules.

The  $RMSD_{bi}$  of these complexes range from a minimum of 2.50 Å for SS16 to a maximum of 4.22 Å for the free peptide,

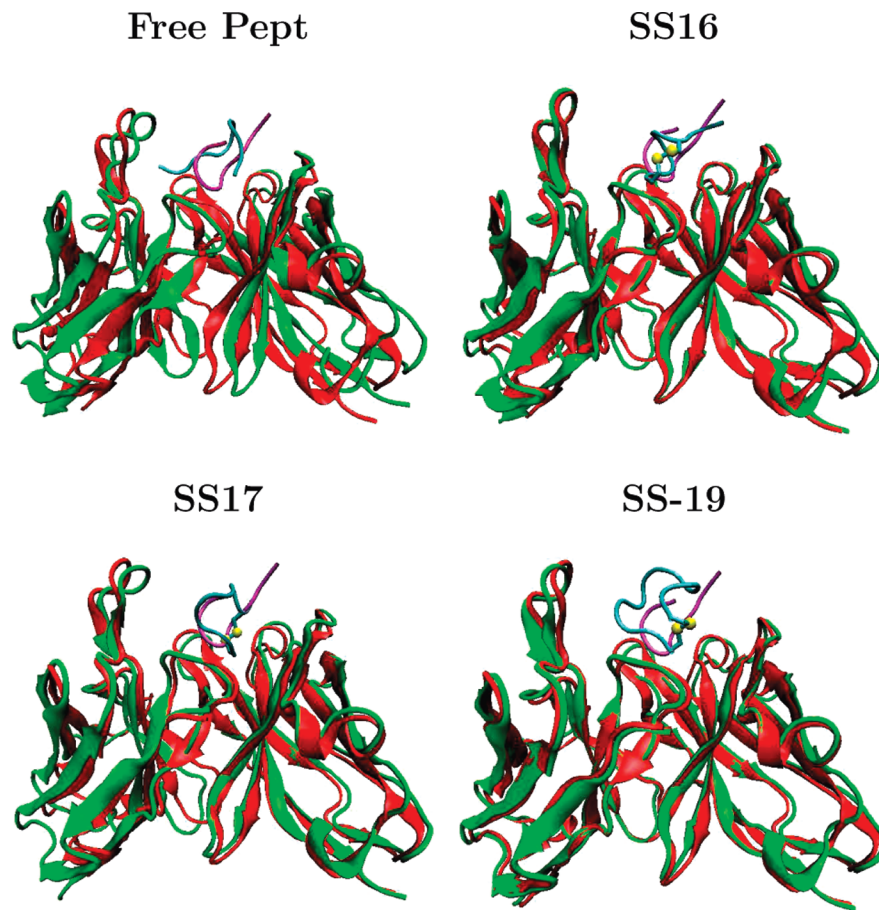


**Figure 6.** Superposition of the lowest-energy structures of the most stable clusters (in green and cyan) with the crystal complex MOG101–108/8-18C5 (in red and magenta). The superposition minimizes the structural distance between the CDR loops of the antibody molecules. The variable domain of the light chain of 8-18C5 is on the left, whereas the IgV domain of the heavy chain is on the right.

passing through values of 2.69, 3.06, and 3.37 Å for SS17, SS07, and SS-19, respectively. These rather high values are due to the fact that the orientation of the peptides is not exactly equal to the crystallographic one. Nevertheless the peptides always occupy the same region of space that the 101–108 fragment occupied in the crystal complex. Moreover, despite the different orientation, the peptides establish with the antibody a significant number of contacts (distance cutoff: 3.5 Å), from a minimum of 47% of the crystallographic contact number in the case of SS17 to a maximum of 64% in the case of SS16 and SS07. An intermediate value of 55% is attained by the free peptide and SS-19. Analysis of Figure 6 also reveals that the binding orientation of the free peptide is rotated by 180° with respect to the crystal fragment 101–108, whereas the disulfide-bonded peptides undergo a rotation of 90°. It follows that the peculiar orientation of fragment 101–108 in the MOG<sup>lgd</sup>/8-18C5 crystal is the result of the steric constraints imposed by the scaffold of the full MOG<sup>lgd</sup> domain. When these restraints are removed, the peptide reorients the apical part of the loop closed by the disulfide bond toward the light chain of the antibody and, in particular, toward the hypervariable loop L1. The fraction of the contacts established with the light chain in fact varies from a negligible 4% in the case of the MOG101–108/8-18C5 crystal to 48.5% and 49.5% in the lowest-energy complexes of SS-19 and SS07 respectively.

Figure 7, based on a contact analysis at a 3.5 Å distance cutoff, summarizes in a very schematic way the most important interactions between the peptides and the antibody.

In agreement with the description in ref 6, in the crystal complex the most important interactions are those established by the N-terminal and C-terminal residues. The long hydrocarbon chain of Arg1 establishes several contacts with the hydrophobic residues of the hypervariable region H1. Since, at physiological pH, Arg1 is likely to be positively charged, it also forms a Coulombic contact with the negatively charged Glu50H situated in CDR H2. Other electrostatic interactions involve the negatively charged Glu7 and Glu8 of the peptide and the positively charged Arg54 and Arg56 belonging to CDR H2. In this respect, it is interesting to notice that MOG 101–108 shows what could be called a *C-terminal redundancy*, being terminated by the triplet Gln6-Glu7-Glu8. In this situation, a rotation displacing e.g. Glu8, could be easily tolerated, since the interactions of this residue would be inherited by Glu7, or, for larger rotations, by Gln6. As already noticed, the free peptide shows an upside-down orientation with respect to the crystal. Despite the 180° rotation, Arg1 approximately occupies the same position occupied in the crystal complex and it therefore retains the same interactions with the hydrophobic residues of CDR H1 and with Glu50H. It is also interesting to notice that, as a consequence of the rotation, the negatively charged Asp2 occupies a location close to the crystallographic position of Glu7 and Glu8 inheriting part of their contacts. Finally, Glu7 and Glu8 can no longer interact with Arg54 and Arg56, because the side chains of these residues are now oriented toward CDR L1, where they interact with Lys30F. Quite surprisingly, the orientation of Glu7 and/or Glu8 remains almost invariant also

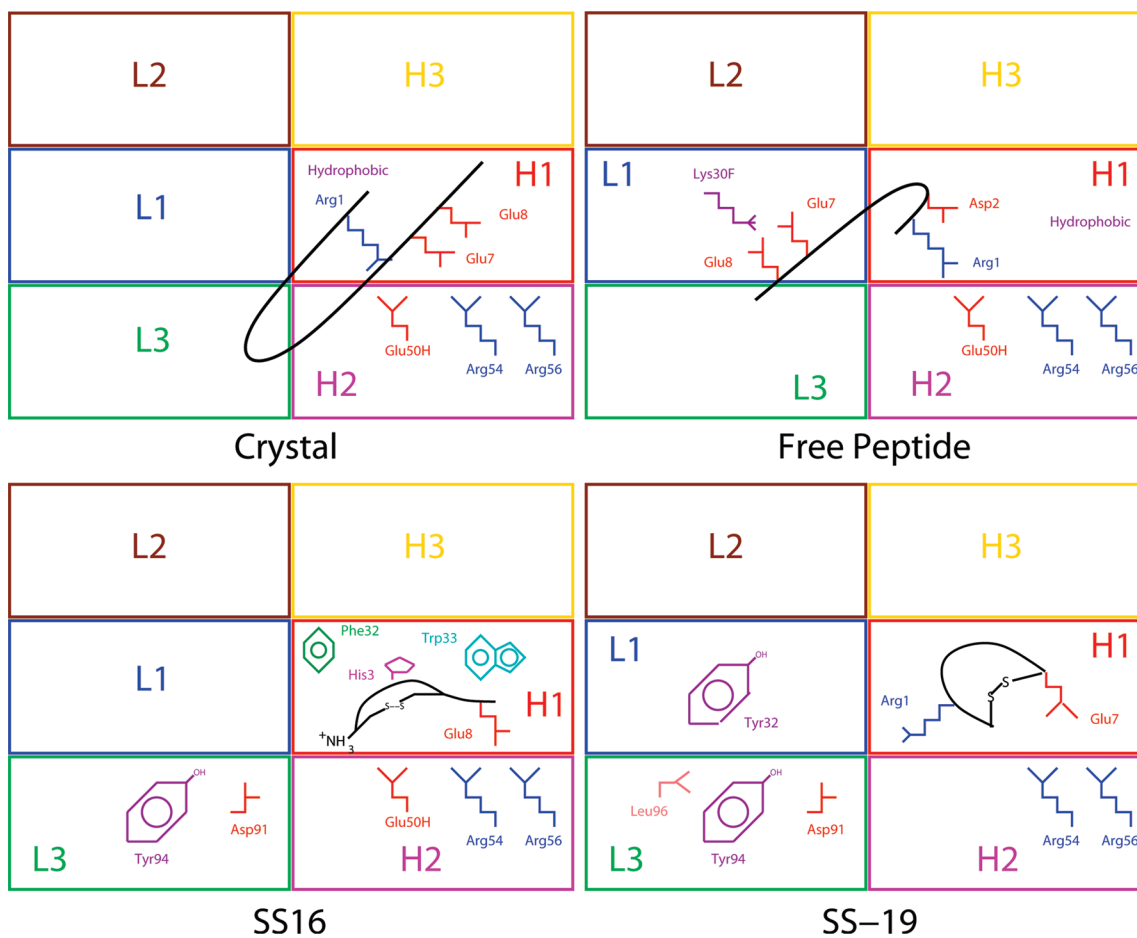


**Figure 7.** Cartoon representation of the bidimensional projection of the interface region of the crystal and lowest-energy peptide/antibody complexes produced by the docking simulations. The binding pocket of the antibody is composed by six rectangles representing the hypervariable regions of the light (L1–L3) and heavy chain (H1–H3) of the antibody. Key contacts have been identified using a distance cutoff of 3.5 Å.

in the binding arrangements of the disulfide-closed peptides despite a rotation of 90°, and therefore the interaction of these acid residues with Arg54 and Arg56 remains a key contribution to the complex stability. In peptide SS16 the amino terminus of the peptide is reoriented toward region L3 where it establishes interactions with the polar Tyr94 and Asp91 residues. Another interesting feature of SS16 is represented by the positions of His3 and Ser4 that are inverted with respect to the positions of the corresponding residues in the crystal. As a consequence, in SS16, His3 is the center of a network of interactions with Phe32 and Trp33 (CDR H1) that in the crystal were established by Ser4. Conversely, in SS16 Ser4 inherits some of the interactions with Thr101 (CDR H3) that in the crystal were established by His3.

Peptides SS17, SS07, and SS-19 have an orientation similar to that of SS16, but the loop stabilized by the disulfide bond here is longer. In SS17 this loop is so long that Ser4 and Gln6 lose the crystallographic contacts, but not long enough to replace them with new contacts established with residues of CDRs L1 and L3. The side chain of Ser4, for example, is oriented toward L3, but it is still so distant that no contact can be made. Peptides SS07 and SS-19 retain Arg1 that is now reoriented toward L1, where it establishes electrostatic interactions with Asp91 (L3) and van der Waals contacts with the aromatic ring of Tyr94 (L3). Due to the longer length of the SS-closed loop, in SS-19 Arg1 also forms contacts with residues of region L1 and in particular with Tyr32.

The information deriving from the contact analysis can be complemented by the data resulting from an analysis of the flexibility of the CDRs and of the peptides during the semi-flexible HADDOCK simulations. Here we only report the main findings, while a detailed discussion can be found in the Supporting Information.

When only backbone atoms are accounted for, the flexibility appears to be maximal in CDR H3, intermediate in CDRs L1, L2, L3, and minimal in regions H1 and H2. This pattern simply reflects the fact that the peptides dock to the antibody in the area of CDRs H1 and H2 so that the residues of these hypervariable loops do not need a deformation of the backbone to enter in contact with the peptides. Conversely, the longer distance of CDRs H3, L1, L2, L3 from the peptide/antibody interface requires a displacement of the backbone to bring these CDRs within interaction distance from the peptide. When the heavy atoms of the side chains are also included into the flexibility analysis, this pattern is confirmed with the only exception that now loop H2 is also highly flexible. This behavior turns out to be determined by the repositioning of the side chains of Arg54(H2) and Arg56(H2) that move closer to their binding partners in the peptides.

The flexibility analysis of the peptides, on the other hand, reveals a high flexibility of the disulfide-linked cysteines of SS16, SS17, SS07, and SS-19. In general, the N-terminal cysteine moves its NH<sub>3</sub><sup>+</sup> group close to a highly polar or negatively charged binding partner. By contrast, the movement

of the second cysteine is usually a passive drag due to the pulling of the first, covalently bonded cysteine. Other flexible residues are *Tyr*5, *Glu*7, and/or *Glu*8 that move closer to their binding partners. As a conclusion, flexibility plays an important role in the optimization of the interaction network in agreement with the observations by Rini et al.<sup>32</sup> on the importance of induced fit as a mechanism for the antibody recognition of  $\beta$ -hairpin peptide antigens.

The conservation of the contact interface in the binding pocket of the 8-18C5 antibody is an important issue. In fact, an efficient competition with MOG<sup>IgG</sup> requires the ability of the peptides to dock in a region as largely overlapping as possible with the crystal binding site. The study of the Buried Surface Area (BSA) and a contact analysis with a cutoff of 3.0 Å shows that *Arg*54(H2) and *Arg*56(H2) are part of the contact interface of all the peptides, where they preferentially interact with *Glu*7 and/or *Glu*8. The interactions established by the two arginines of CDR H2 are strengthened by the neighboring residues *Glu*50(H) and *Leu*52(H) that play an ancillary role. Another couple of residues present in the binding sites of the complexes with all variants of MOG 101–108 includes *Thr*97(H3) and *Met*98(H3) whose action is complemented by the neighboring *Gly*95(H), *Asn*96(H), and *Asn*100(H) residues.

The residues of CDRs L1 and L3 are extremely important in the binding site of the complexes with SS07 and SS-19, while they make fewer contacts with the crystal fragment, the free peptide, and peptides SS16 and SS17 where the loop closed by the disulfide bond is absent or shorter and it is more difficult for the peptide to enter in contact with the light chain of the antibody. In particular, residues *Asn*30D(L1), *Lys*30F(L1), and *Tyr*32(L1) as well as residues *Asp*91(L3), *Tyr*94(L3), and *Leu*96(L3) play a negligible role or no role at all in the crystal complex, while they are present in the binding site of all the other peptides and are particularly important in the binding interface of SS07 and SS-19 (with a preference of SS07 for interactions with CDR L1 and a preference of SS-19 for contacts with CDR L3). By contrast, still due to the length of the disulfide-closed loop, residues *Ser*31(H1), *Phe*32(H1), and *Trp*33(H1) play a crucial role in the binding site of the crystal fragment, the free peptide, and peptides SS16 and SS17, while they are not part of the binding site of peptides SS07 and SS-19.

Despite the differences therefore, a significant overlap exists among the binding site of the crystal complex and those recognized by the derivatives of MOG 101–108. A more detailed analysis, together with tables of residue interaction and BSA, is provided in the Supporting Information.

### 3. Discussion

In this paper we have studied a potential role of fragment 101–108 of MOG<sup>IgG</sup> as a blocking agent of the binding site of the MS-associated autoantibody 8-18C5. It is a current opinion<sup>4,5</sup> that the epitopes recognized by MOG-specific demyelinating antibodies are conformation-dependent, whereas antibodies against linear epitopes of MOG do not induce widespread demyelination.<sup>33</sup> These studies, however, were conducted before

the 3D-structure of the MOG<sup>IgG</sup>/8-18C5 complex was resolved.<sup>6</sup> The crystal structure of the complex reveals a surprisingly dominant contribution of MOG<sup>IgG</sup> fragment 101–108 that we confirmed through an alanine scanning computation showing that five out of eight residues in this fragment can be classified as hot spots. As pointed out in ref 6, a possible explanation of the failure of previous studies to identify this linear epitope may rely on the relaxation of the strained conformation of *His*103 when fragments including this residue are excised from the scaffold of MOG<sup>IgG</sup>. Another even simpler explanation is that the epitope mapping of MOG<sup>IgG</sup> was accomplished with peptides that, being too long (15 to 25 residues), folded into a structure sterically incompatible with the binding pocket of 8-18C5. The importance of fragment 101–108 of MOG<sup>IgG</sup> on the other hand is also suggested by its sequence similarity with a subsequence of protein CT863 of *Chlamidia pneumonia* and *Chlamidia trachomatis*, microorganisms previously associated with MS, which suggests the pathogenesis of this disease to be based on a phenomenon of molecular mimicry.<sup>6</sup>

The ability of the excised 101–108 fragment to recognize the binding site of 8-18C5 when kept in the crystal-like conformation suggested the working hypothesis that if peptide 101–108 retains a crystal-like structure after equilibration under physiological conditions, then it might be able to fit into the binding pocket of the autoantibody. Our hypothesis proved to be only partially correct. On the one hand, our REMD simulations showed the existence of a significant proportion of crystal-like structures in the equilibrium population (50% of the conformations is less than 3.0 Å *RMSD*<sub>backb</sub> away from the crystal fragment). On the other hand, the free peptide does not bind to the ligand pocket of 8-18C5 in the crystallographic orientation and the binding performances of the disulfide-closed analogues do not follow the ranking of their native-likeness. In particular, we found that the best binding behavior was exhibited by peptide SS16, one of the least crystal-like compounds we tested. This apparent paradox can be easily explained. If the peptide could very faithfully retain the crystal structure, as is the case for our semiflexible docking simulations using the crystal fragment, then it would dock to the antibody in the crystal orientation. All the equilibrated peptides, however, bear just a rough resemblance to the crystal fragment, and they therefore fit into the binding pocket in an alternative, noncrystallographic orientation. In this situation the best ligand may be represented by a peptide not particularly crystal-like but endowed with a structure complementary to the binding site in the new arrangement. Nevertheless, the stability of the peptide/antibody complexes, and the fact that the peptides occupy the same region of space that the 101–108 fragment occupied in the crystal, supports the possibility of using these compounds as blocking agents of the 8-18C5 autoantibody. As a conclusion, even if experimental tests are strongly required, we believe that fragment 101–108 and its analogues represent a good starting point for the development of therapeutic and diagnostic tools for MS.

### 4. Materials and Methods

**4.1. Histidine Protonation.** The protonation state of *histidine* residues is a rather critical issue since this may significantly affect the equilibrium conformation adopted by small peptides. Moreover,

- (30) Wang, J.; Cieplak, P.; Kollmann, P. A. *J. Comput. Chem.* **2000**, 21, 1049–1074.  
 (31) Onufriev, A.; Bashford, D.; Case, D. A. *Proteins: Struct., Funct., Bioinf.* **2004**, 55, 383–394.  
 (32) Rini, J. M.; Schultze-Gahmen, U.; Wilson, J. A. *Science* **1992**, 255, 959–965.

- (33) von Büdingen, H. C.; Hauser, S. L.; Fuhrmann, A.; Nabavi, C. B.; Lee, J. I.; Genain, C. P. *Proc. Natl. Acad. Sci. U.S.A.* **2002**, 99, 8207–8212.

due to the importance of electrostatic interactions, *His* protonation states may also influence the final arrangement of a ligand in the binding site of a macromolecule. In the MOG<sup>1<sup>ed</sup></sup>/8-18C5 crystal complex, two *His* residues are located in the interaction interface: *His*92 is part of CDR L3 while *His*103 is on the tip of the FG loop of MOG, i.e. in the 101–108 fragment which is the object of our investigation. The protonation state of *His*92(L3) and *His*103(MOG) (the  $\epsilon$ -tautomer in both cases) was determined using the method proposed by Signorini et al.<sup>34</sup> Such results were confirmed by an analysis performed on the WHAT IF Web Interface (<http://swift.cmbi.ru.nl/servers/html/index.html>). Further details are provided in the Supporting Information.

**4.2. Implicit-Solvent REMD Simulations.** REMD simulations have been performed with the Amber 9<sup>35</sup> suite of programs using the force field ff99SB<sup>29</sup> and the GB continuum solvent model (ref 21) with a 0.2 M concentration of monovalent ions. The MOG 101–108 peptide, built in the extended conformation, underwent 200 steps of steepest descent followed by 200 steps of conjugate gradient minimization. The disulfide-closed peptides were prepared by manipulating, with the MOLDEN program,<sup>36</sup> the crystal fragment MOG 101–108 excised from chain J of the PDB entry **PDB-ID:1PKQ**, and they were then minimized with the same protocol used for the free peptide. Copies (12) of the minimized structures were then created and gradually heated to the chosen temperatures of the REMD protocol in 5 ns employing a time step of 1 fs. The temperature control was attained using the Langevin dynamics with a collision frequency of 1.0 ps<sup>-1</sup>. For each replica a different seed of the random number generator was provided. No cutoff has been used for the nonbonded interactions. A 32-ns REMD simulation was then run. Temperature exchanges were attempted every 2.5 ps which resulted in an average success rate of 48%. The high acceptance ratio is an indication of the fact that the number of temperatures is sufficient for an efficient performance of the REMD algorithm. Moreover, the acceptance ratios are uniform for all pairs of neighboring temperatures (variance: 0.00023) thus allowing a free random walk in the space of temperature. The first 2 ns of the REMD simulation were discarded, and the analysis was performed on 1000 structures uniformly sampled over the last 30 ns.

**4.3. Docking Simulations.** The coordinates of the variable domains of the 8-18C5 antibody were taken from chains F and G of PDB entry **PDB-ID:1PKQ**, truncated in correspondence to Arg108 and Ser113 respectively. Six semiflexible loops were defined, corresponding to the CDRs of the antibody: L1 = {Ser26, Gln27, Ser28, Leu29, Leu30, Asn30A, Ser30B, Gly30C, Asn30D,

Gln30E, Lys30F, Asn31, Tyr32}; L2 = {Ile48, Tyr49, Gly50, Ala51, Ser52, Thr53, Arg54}; L3 = {Asn90, Asp91, His92, Ser93, Tyr94, Pro95, Leu96, Thr97}; H1 = {Phe29, Ser30, Ser31, Phe32, Trp33, Ile34, Glu35, Trp36}; H2 = {Pro52A, Gly53, Arg54, Gly55, Arg56}; H3 = {Thr97, Met98, Val99}. The full peptide to be docked was also defined as a single semiflexible loop. Random Ambiguous Interaction Restraints were then defined by HADDOCK by randomly choosing solvent-exposed residues in the semiflexible regions. Default parameters were used for the HADDOCK run. A total of 1000 initial docked structures were generated. The 200 with the lowest energy were refined using simulated annealing followed by water refinement, and they were finally subjected to clustering and structural analysis.

**4.4. Quality Threshold Clustering.** The algorithm first computes a matrix of pairwise rmsd distances for all couples of structures of the population. In the case of the peptides, the superposition and rmsd computation are both performed using backbone atoms. A cutoff of 3.5 Å is chosen. In the case of peptide/antibody complexes, the structures are superimposed so as to minimize the distance between the backbone atoms of the CDR loops of the antibody. The rmsd is then computed using only the backbone atoms of the peptide, which results in the choice of a rather high cutoff (12.5 Å). The algorithm then builds a candidate cluster for each structure of the population. The distance between any two structures in the cluster must be lower than the chosen cutoff. Only the largest candidate cluster is retained, and the list of structures is updated by removing the structures included in the newly generated cluster. The procedure is recursively repeated until the population list is empty.

**Acknowledgment.** This work was supported by the Italian Ministry of University and Research (Projects of Scientific and Technological Cooperation with the Harvard Medical School within the framework of the Italy-USA bilateral agreements. Protocol Number: RBIN04TWKN. National Coordinator: Prof. Anna Maria Papini). We gratefully acknowledge CINECA and CNR-INFN Iniziativa Calcolo per la Fisica della Materia for the allocation of computer time. Gratefulness is also expressed to ENEA for allowing access to the high-performance architectures of the CRESCO (Computational Research Center for Complex Systems) Project.

**Supporting Information Available:** The main topics discussed in the Supporting Information are (1) Histidine Protonation, (2) Implicit vs Explicit Solvent Simulations, (3) Clustering Consistency Analysis, (4) Binding Site Conservation, (5) Semiflexibility Analysis. This material is available free of charge via the Internet at <http://pubs.acs.org>.

JA905154J

(34) Signorini, G. F.; Chelli, R.; Procacci, P.; Schettino, V. *J. Phys. Chem.* **2004**, *108*, 12252–12257.

(35) Case, D. A. *AMBER 9*, University of California: San Francisco, 2006.

(36) Schaftenaar, G.; Noordik, J. K. *J. Comput.-Aided Mol. Des.* **2000**, *14*, 123–134.